Effect of Waveforms on Morphology Development in Chaotic Mixing of Polymers

Madhusudan Sau and Sadhan C. Jana
Dept. of Polymer Engineering, University of Akron, Akron, OH 44325

DOI 10.1002/aic.10198
Published online in Wiley InterScience (www.interscience.wiley.com).

The effect of waveforms of rotor motion in a chaotic mixing device on the development of morphology in the blending of polypropylene (PP) and polyamide 6 (PA6) was investigated. The rotor motion was delivered in a steady and time-periodic manner and the mixing effectiveness was evaluated in terms of Poincaré maps and stretching distribution, the speed of conversion of PP-phase into droplets, and droplet size distribution. The pathway of morphology development, such as deformation of the PP-phase into lamella, fibrils, and droplets, was found not to depend on the nature of the waveform. However, the makeup of each morphological form depended strongly on the particular waveform used. The best results were obtained when the rotor motion was delivered using a sine waveform. In this case, the PP-phase turned most rapidly into fibrils and droplets and the droplets were of more uniform size. The square waveform, although produced higher mean stretching and showed more uniform mixing in Poincaré maps, yielded large-size droplets, purportedly through premature breakup of the fibrils in the zones of weak flow, such as in the vicinity of the stationary rotors. © 2004 American Institute of Chemical Engineers *AIChE J,* 50: 2346–2358, 2004
Keywords: waveforms, morphology, chaotic mixing, immiscible polymers, fibrillar

Introduction

In the blending of immiscible polymers in screw extruders, the microstructure is created from the interplay of processing parameters, such as rates of shear, total strain, frequency of flow reorientation, and material parameters, including interfacial tension, viscosity, relaxation modulus, and composition of the phases. Early in mixing, as in the case of viscous, miscible liquids, the fluid domains are deformed to produce three-dimensional (3-D) lamellar structures (Ghosh et al., 1991; Kwon and Zumbrunnen, 2001; Lindt and Ghosh, 1992; Lyngaae-Jorgensen, 1996; Scott and Macosko, 1991, 1995; Sundararaj et al., 1992, 1995; Vanoene, 1972), characterized by the thickness of individual lamella along a cross-sectional plane, defined as *striation thickness* (Ottino et al., 1979). The goodness of mixing, at this stage, is defined in terms of a striation thickness distribution. In common mixing flows, such as shear flows encountered in single- and twin-screw extruders, the striation thickness decreases linearly with time (Erwin, 1978a,b), whereas in chaotic mixing flows generated by time-periodic motion of boundaries (Aref, 1984; Jana et al., 1994a; Leong and Ottino, 1989; Niederkorn and Ottino, 1993; Ottino, 1989; Swanson and Ottino, 1990) or spatially periodic variation of flow-channel geometry (Jana et al., 1994b; Jones et al., 1989; Kim and Kwon 1996a,b; Kusch and Ottino, 1992) the striation thickness reduces exponentially rapidly with time.

In the case of immiscible polymers, the lamellar structures with associated striation thickness distribution undergo interfacial instabilities beyond a "critical lamella thickness," produce periodic distortions in a preferential direction, and eventually disintegrate into fibrillar structures (Ghosh et al., 1991; Lyngaae-Jorgensen, 1996). The fibrils, in turn, undergo capillary instability and break up into droplets and the newly formed droplets, if larger than a critical size, may repeat the breakup process. A pseudo-equilibrium state is finally reached describing a somewhat stable morphology from the balance of inter-

Correspondence concerning this article should be addressed to S. C. Jana at janas@uakron.edu.

facial and viscous forces and from the competing rates of breakup and coalescence (Chesters, 1991; Jenssen and Meijer, 1995). Note that the lamellar structures of miscible liquids do not undergo such distortion and repetitively form thinner striations until molecular diffusion takes over to homogenize the system.

The features of morphology development described above for screw-extrusion processes immediately relate to self-similar mixing structures produced in chaotic mixing of polymers. In this context, an immiscible dispersed phase subjected to chaotic mixing flow may deform exponentially rapidly and produce very thin, self-similar lamellar structures, which may undergo instabilities and break up into fibrils of very high aspect ratio and droplets of very small diameter. Note that the deformation of fluid domains into lamellar structures by chaotic mixing and stretching and breakup of liquid filaments in chaotic flow follow self-similarity (Muzzio et al., 1991a,b); other attributes of self-similarity of chaotic mixing have been investigated in the context of hydrodynamics-aided chemical reactions (Metcalfe and Ottino, 1994; Muzzio and Liu, 1996; Szalai et al., 2003) and microstructure development in miscible fluids (Galaktionov et al., 2002; Kruijt et al., 2001). Zumbrunnen and coworkers (Kwon and Zumbrunnen, 2001; Liu and Zumbrunnen, 1999; Zumbrunnen and Chibber, 2002; Zumbrunnen and Inamdar, 2001; Zumbrunnen et al., 1996) studied blending of polymers by chaotic mixing, using two designs of batch chaotic mixing devices such as a 3-D cavity and a journal bearing and one continuous chaotic mixing device. In these studies, the motions of rotating elements were delivered in square waveform and various structures were produced, such as lamella, fibrils, droplets, and their combinations. These authors studied blending of polystyrene (PS) with low-density polyethylene (LDPE) (Kwon and Zumbrunnen, 2001; Liu and Zumbrunnen, 1999; Zumbrunnen and Chhiber, 2002), polypropylene (PP) with ethylene propylene diene monomer (EPDM) (Zumbrunnen and Inamdar, 2001), and polyethylene vinyl acetate (EVA) with LDPE (Zumbrunnen et al., 1996). These studies established that the pathway of morphology development in chaotic mixing of immiscible polymers is similar to those observed in screw extrusion (Ghosh et al., 1991; Sundararaj et al., 1995). However, the lamellas and fibrils were found to persist over longer periods of time, although the strain rates used by Zumbrunnen and coworkers were much smaller: 0.07–2.75 (1/s) in Zumbrunnen and Chhiber (2002), compared to typically about 50 (1/s) encountered in screw extrusion. Despite such research activities, many relevant issues have not been explored in the context of chaotic mixing of polymers.

One such issue is related to mixer designs, including the production of uniform stretching of material interfaces and production of uniform drop size distribution. These can be achieved by designing mixers that eliminate the zones of weak flows so as to avoid early breakup of extended fibrils. It is known that breakup of extended fibrils in low stretching zones results in larger droplets (Tjahjadi and Ottino, 1991). Another issue is to assess the influence of chaotic mixing parameter, which takes into account the frequency of oscillation of the time-periodic flow field, on morphology development. An understanding of the effects of various time-periodic waveforms on morphology development is also necessary for scale-up and optimization of batch and continuous chaotic mixing devices. These issues must be resolved before the potential of chaotic mixing can be fully realized, as in the design of new mixing equipment or in the retrofitting of the existing ones.

We undertook a study in our laboratory to investigate the development of morphology in the blending of a shear-thinning polymer (PP) with a Newtonian polymer (PA6) in a chaotic mixing device. The results of the effects of mixer designs and chaotic mixing parameter θ (angular displacement per period) on the pathway of morphology development and droplet size distribution were reported elsewhere (Sau and Jana, 2004). It was found that for a sine waveform, a value of $\theta = 1440°$ provided the best results in terms of uniformity of mixing and fastest development of morphology in the blending of PP with PA6. A highly stretched fibrillar form of the PP-phase with aspect ratio of about 10,000 was found, which at later stages of mixing stretched further and broke up into droplets, about 99% of which fell well below the equilibrium size. In another study (Jana and Sau, 2004), it was found that the speed of the morphological transitions slowed significantly when the dispersed phase was of higher viscosity. In addition, it was shown that the droplet size distribution did not follow self-similar scaling features. In this report, complete results on the effects of time-periodic waveforms on morphology development in PP–PA6 system are presented. We exploited the Newtonian nature of the matrix polymer PA6 to compute the stretching distributions and Poincaré maps and arrived at some distinguishing features of the various waveforms used.

Experimental

Materials

Polyamide 6 (Zytel® 7301 NC010, supplied by DuPont, Wilmington, DE) and polypropylene (melt flow index 5.0, supplied by Equistar Chemicals, Houston, TX) were considered as immiscible polymers for the study. The crystalline melting points of PA6 and PP were found to be 220 and 165°C, respectively, from differential scanning calorimetry (DSC). The composition of the blend was maintained at 90% by weight of PA6; PA6 formed the continuous phase. The steady shear viscosities of the polymers were determined by an ARES Rheometrics (Rheometrics/TA Instruments, New Castle, DE) cone and plate rheometer and Instron (Canton, OH) capillary rheometer as presented in Figure 1 at the mixing temperature of 250°C; the ratio of zero shear viscosities of PP and PA6 was found to be 9.8. The interfacial tension (σ) between PA6 and PP was determined by the thread breakup method (Chappelear, 1964; Elemans et al., 1990) and found to be 0.0126 N m^{-1} at 250°C.

Chaotic mixing device

PP and PA6 were mixed in chaotic flow produced in a batch chaotic mixer (Sau, 2003; Sau and Jana, 2004) by time-periodic variation of rotor speeds. The cross-sectional shape of the mixing chamber (Figure 2) is similar to that of twin-screw extruders and was chosen to eliminate the zones of very low stretching; zones of low stretching are known to promote premature breakup of fibrils into larger-size droplets (Kang et al., 1996; Tjahjadi and Ottino, 1991) and to result in wider drop size distribution.

The shear gap (d) between the stationary walls (Figure 2)

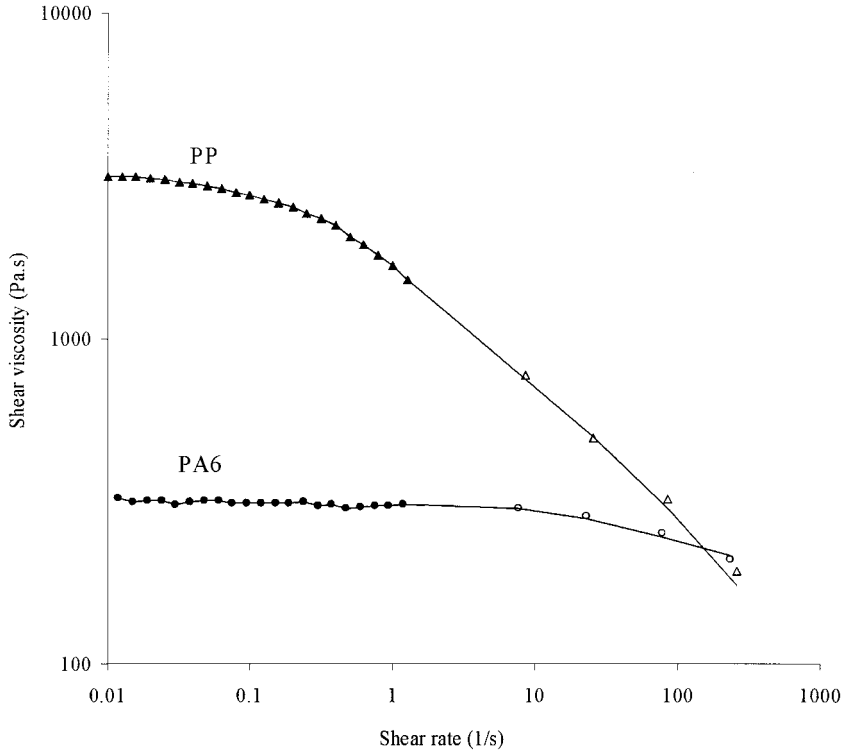

Figure 1. Shear viscosity of PP and PA6 at 250°C.

Filled symbols represent data from cone-plate rheometer and open symbols represent data from capillary rheometer. Solid lines represent interpolation of data points.

and the rotors was maintained at 0.0127 m using two circular rotors of 0.0254 m diameter. This shear gap is much larger than about 0.0035 m, observed for 30-mm Coperion/Werner & Pfleiderer twin-screw extruders (Coperion Corp., Ramsey, NJ). The depth of the mixing chamber was 0.0127 m. For this geometry, approximately 33 gm of mixed materials were produced from one batch experiment.

Waveforms

Intuitively, too frequent and too slow change of speed of rotors is not useful in producing uniform and widespread mixing. Moreover, the waveforms with high frequency are difficult to achieve in actual operation because of machine limitations, such as eddy currents of motors, which can cause unnecessary warming. On the other hand, a slow speed variation limits chaotic mixing to a narrow band near the homoclinic orbit (Jana et al., 1994a; Kaper and Wiggins, 1993); thus global mixing cannot be achieved with slow speed variation. Prior work (Chien et al., 1986) has shown that at an optimum frequency of oscillation, the interfacial area between two miscible fluids grows at the fastest rate. In addition, different single-frequency waveforms have been shown to produce qualitatively similar lamellar structures in miscible liquids, once the perturbation parameter was adjusted to give the same leading term in Fourier series or the same average deviation from the mean speed (Jana et al., 1994a; Swanson, 1991). However, as will be seen later, significantly different results were obtained in the blending of immiscible polymers by varying the nature of waveforms.

The speeds of rotors A and B were varied in steady (Case 1) and time-periodic fashion following three time-periodic waveforms: sine (Case 2), square (Case 3), and a combination of steady and sine waveforms (Case 4), as shown in Figure 3.

Case 1. Steady Motion

$$\Omega_A = \Omega \qquad \Omega_B = \Omega \tag{1}$$

Case 2. Sine Waveform

$$\Omega_A = \frac{\Omega}{2}\left(1 + \varepsilon \cos\frac{2\pi t}{T}\right) \qquad \Omega_B = \frac{\Omega}{2}\left(1 - \varepsilon \cos\frac{2\pi t}{T}\right)$$

$$0 \le t \le T \tag{2}$$

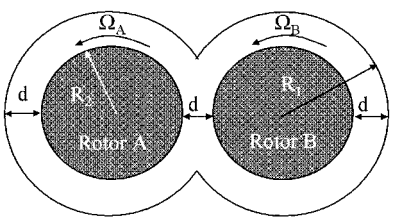

Figure 2. Cross-sectional view of the mixing device.

R_1 is the radius of the chamber wall, R_2 is the radius of rotor, d is the gap size, and Ω_A and Ω_B are angular speeds of rotors A and B, respectively.

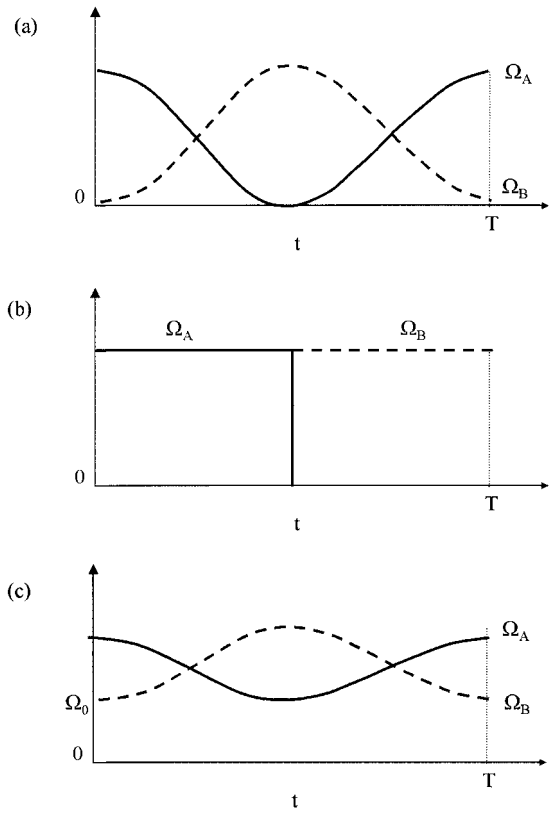

Figure 3. Different waveforms.

(a) Sine, (b) square, and (c) combination of steady and sine waveforms.

Case 3. Square Waveform

$$\Omega_A = \frac{\Omega}{2}(1+\varepsilon) \qquad \Omega_B = \frac{\Omega}{2}(1-\varepsilon) \qquad 0 \le t \le \frac{T}{2}$$
$$\Omega_A = \frac{\Omega}{2}(1-\varepsilon) \qquad \Omega_B = \frac{\Omega}{2}(1+\varepsilon) \qquad \frac{T}{2} < t \le T \tag{3}$$

Case 4. A Combination of Steady and Sine Waveform

$$\Omega_A = \Omega_0 + \frac{\Omega}{4}\left(1 + \varepsilon \cos\frac{2\pi t}{T}\right)$$
$$\Omega_B = \Omega_0 + \frac{\Omega}{4}\left(1 - \varepsilon \cos\frac{2\pi t}{T}\right) \qquad 0 \le t \le T \tag{4}$$

In Eqs. 1–4, ε is a perturbation parameter, which measures the deviation from the mean speed; Ω_A and Ω_B are, respectively, the angular speeds of rotors A and B; and T is the time period. Note that the rotors were rotated in the same direction, but their speeds were varied according to Eqs. 1–4. The term Ω_0 denotes the steady portion of the rotor speed in Eq. 4 and Ω denotes the peak rotor speed. The value of the chaotic mixing parameter θ was obtained using Eq. 5 and was kept the same in each case by adjusting the values of T.

$$\theta = \int_0^T \Omega_A(t)dt = \int_0^T \Omega_B(t)dt \tag{5}$$

Shear rate

Two issues were encountered in the implementation of various waveforms. First, for a given rotor speed, the value of shear rate ($\dot{\gamma}$) was not constant in the gap and varied from its highest value at the rotor surface to the lowest at the chamber wall. This was attributed to the larger size of the mixing gap compared to the diameter of the rotors. Second, the adjustment of the value of perturbation parameter ε in Eqs. 1–4 to give the same deviation from the mean speed or to give the same leading term in the Fourier series, as presented by Jana et al. (1994a), leads to different values of peak speed Ω for different waveforms. For example, $\varepsilon = 8/\pi^2$ for sine waveform and $\varepsilon = 2/\pi$ for square waveform provided the same lead term in the Fourier series and produced qualitatively similar lamellar structures in the mixing of miscible liquids (Jana et al., 1994a). However, implementation of these values of ε led to differences in shear rates at the rotor surfaces among different waveforms. Consequently, the shear viscosity value of PP at the rotor walls also changed for various waveforms. To avoid this, the value of ε was adjusted to unity, such that the values of peak rotor speed and the peak shear rate at the rotor surfaces remained the same in all cases.

The value of peak rotor speed Ω was chosen to be 0.14 m/s, which gave values of peak shear rate at the rotor surface and at the chamber walls of, respectively, 17.7 and 7.1 s^{-1}. In the case of combined waveform (Eq. 4), this was met by maintaining $\Omega_0 = \Omega/2$. The apparent peak shear rate, defined as the ratio of peak speed and the mixing gap (d) was found to be 10.6 s^{-1}. Accordingly, the time-averaged shear rates (over one time period T) at the rotor surface ($\dot{\gamma}_{rotor}$) and at the chamber walls were calculated to be, respectively, 8.8 and 3.5 s^{-1} in all cases.

In line with an optimum frequency of oscillation found by Chien et al. (1986), a value of $\theta = 1440°$ was chosen in all experiments and computations because it produced widespread mixing in the mixing chamber (Sau, 2003; Sau and Jana, 2004). A value of $T = 4.7$ s was chosen to obtain $\theta = 1440°$ in Cases 2–4. The value of total strain (γ) was calculated from Eq. 6

$$\gamma = nT\dot{\gamma}_{rotor} \tag{6}$$

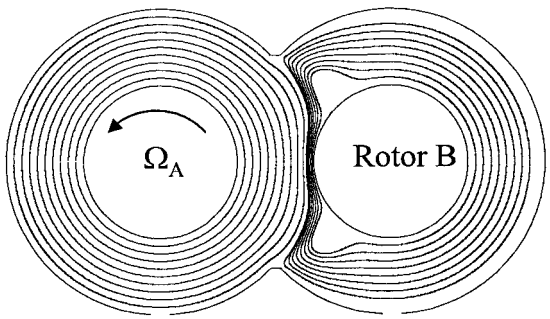

Figure 4. Steady streamline portraits for rotation of Rotor A with Rotor B stationary.

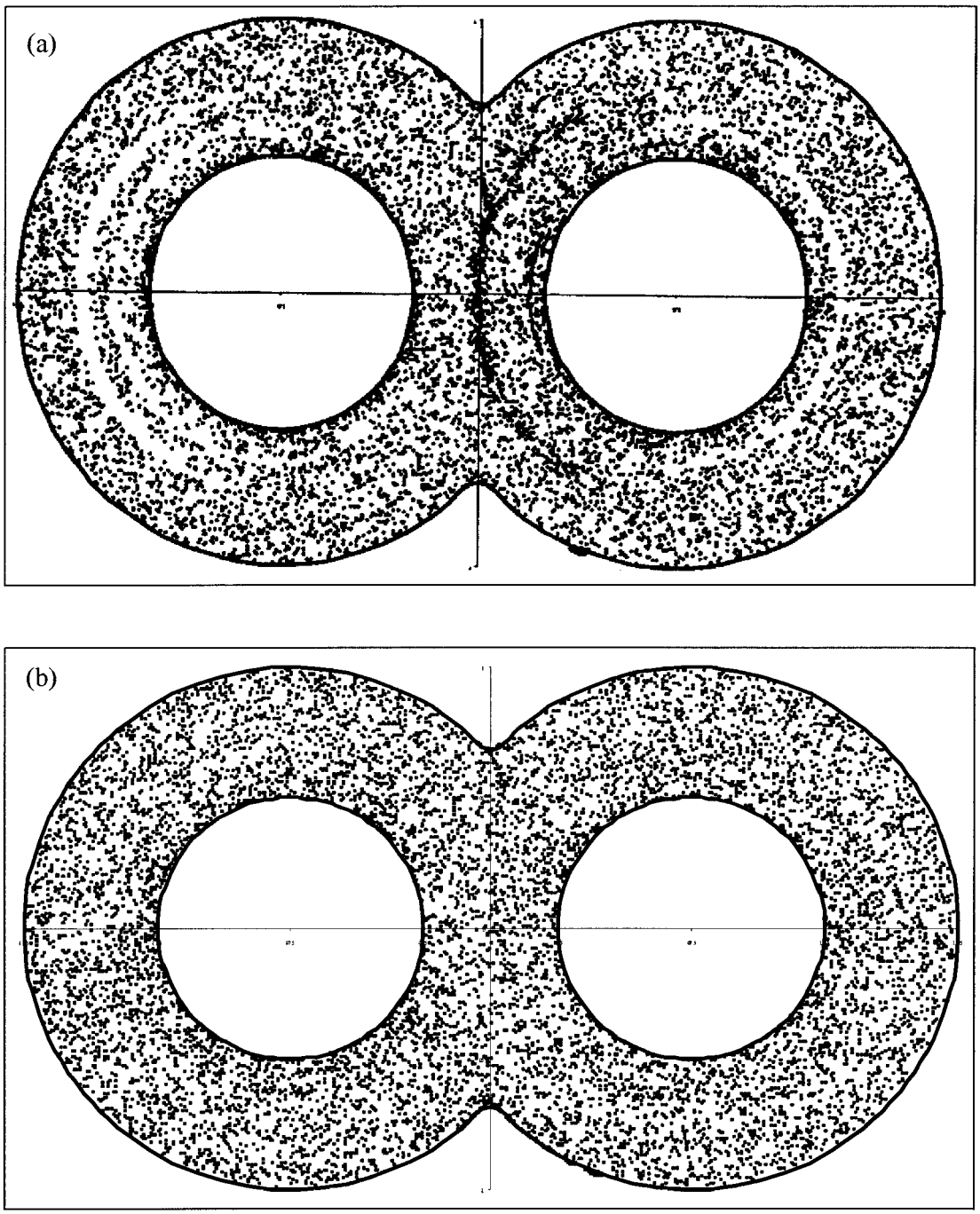

Figure 5. Poincaré maps for $\theta = 1440°$.

(a) Sine waveform (Case 2), (b) square waveform (Case 3), and (c) combination of sine and steady (Case 4).

where n is the number of periods of periodic waveform. For steady motion, the product nT was replaced by the total time of experiment t.

The shear viscosity of the PP-phase varied from 3137 Pa s at $\dot{\gamma} = 0\ s^{-1}$ to 850 Pa s at $\dot{\gamma} = 6.2\ s^{-1}$ to 800 Pa s at $\dot{\gamma} = 7.1\ s^{-1}$ to 600 Pa s at $\dot{\gamma} = 17.7\ s^{-1}$ (Figure 1). Thus, the viscosity ratio (p) of PP and PA6 changed from 9.8 at $\dot{\gamma} = 0\ s^{-1}$ to 2.6 at $\dot{\gamma} = 6.2\ s^{-1}$ to 2.5 at $\dot{\gamma} = 7.1\ s^{-1}$ to 1.8 at $\dot{\gamma} = 17.7\ s^{-1}$.

Mixing experiments

PP and PA6 were available in the form of pellets of approximately 0.002 m in diameter and 0.004 m in length. Pellets were added into the narrowest zones between the rotors (Figure 2) to form a block of $0.0127 \times 0.0354 \times 0.0127$ m. The rest of the mixing chamber was filled with PA6 pellets. The polymers were allowed to melt at 250°C with the aid of a 1000-W band heater surrounding the mixing chamber. The vertical

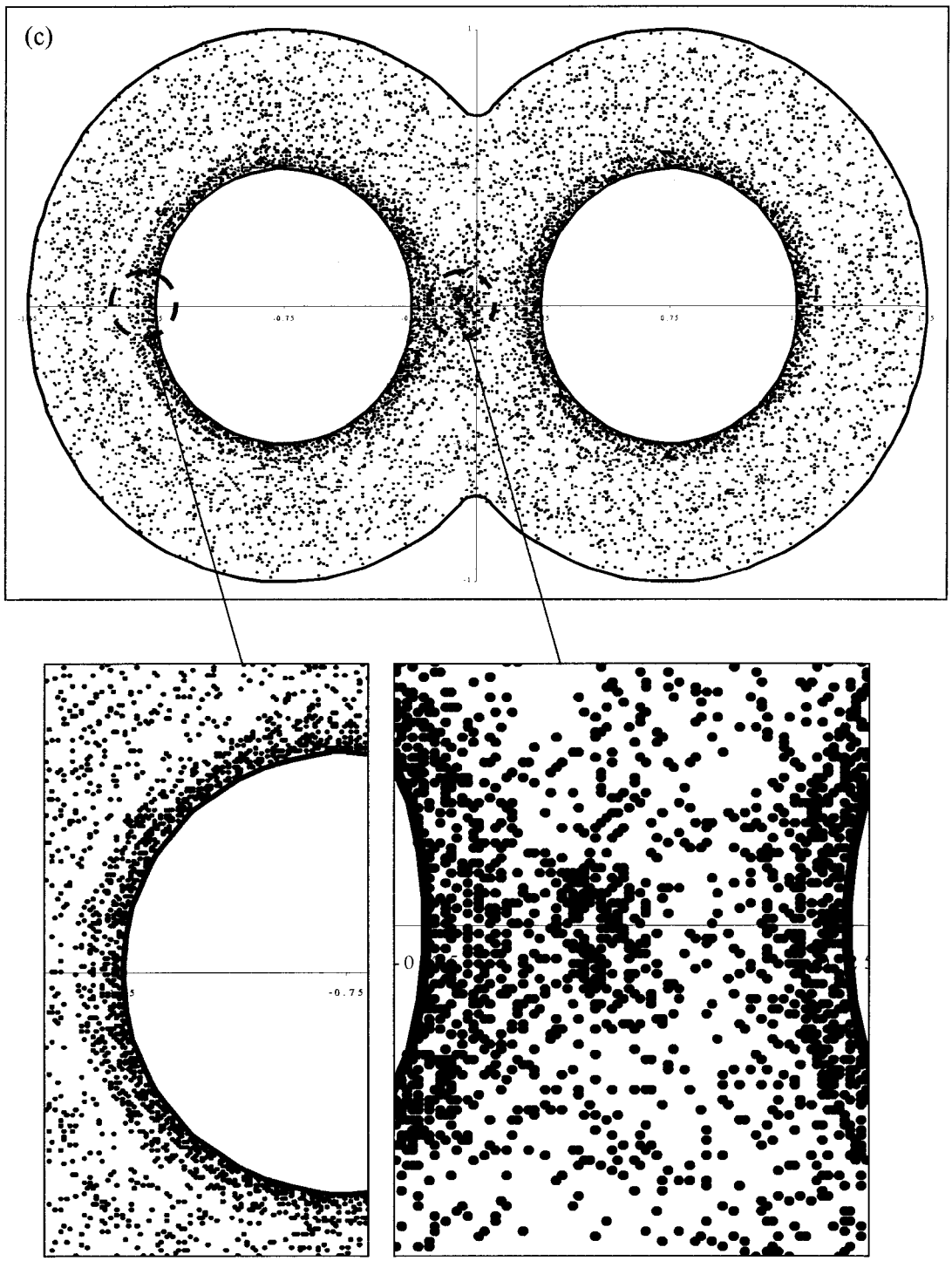

Figure 5. (continued)

placement of the rotors and the mixing chamber facilitated complete segregation of the polymer melt until mixing began. Polymers were mixed for a desired total strain (γ) and cooled in a bath of iced water. The total times for cooling of the system to below the melting point of PP and to room temperature were approximately 30 s and 3 min.

The morphology of the PP-phase was revealed by dissolving the PA6-phase in formic acid in a Soxhlet extraction setup. The droplets of the PP-phase were retained in a ceramic thimble with nominal pore diameter of 0.1 μm. The morphology of the PP-phase was examined by optical and scanning electron microscopy (SEM). The distribution of size of the PP-phase was obtained from several SEM images of the same sample specimen and was analyzed using Scion Image image-analysis software (version 4.0.2, Scion Corp., Frederick, MD).

Poincaré maps and stretching calculations

Poincaré maps and stretching values were calculated on the assumption that the presence of 10 wt. % of PP did not alter the flow very significantly. Moreover, such calculations were expected to yield only some qualitative distinguishing features (such as the existence of islands) of bulk mixing in the mixing device as a function of various waveforms. However, a more quantitative comparison of the effects of waveforms must be based on Poincaré maps computed for the experimental system, which takes into account the presence of the PP-phase in the flow. Under the assumption stated above, the equations of motion of a fluid element at position $\mathbf{x}$ at any time t are given in terms of the velocity $\mathbf{v}$ as follows

$$\frac{d\mathbf{x}}{dt} = \mathbf{v}(\mathbf{x}, t) \tag{7}$$

$$\text{I.C.: } \mathbf{x} = \mathbf{X} \qquad \text{at } t = 0 \tag{8}$$

The velocity field $\mathbf{v}(\mathbf{x}, t)$ was computed using boundary integral equation methods (Higdon, 1985). Figure 4 presents a streamline portrait of steady flow obtained by rotating Rotor A. The fluid element trajectories were obtained by integration of Eq. 7. The streamline portrait for steady rotation of Rotor B is the mirror image of Figure 4 about the y-axis. A series of intermediate streamline portraits are possible for this flow if one considers the time-periodic variation of the ratio of rotor speeds as given in Eqs. 2 and 4 (Jana et al., 1994a). However, these were not computed.

Poincaré maps were obtained using Eq. 7. The value of stretching ratio (λ) at a location $\mathbf{X}$ in the mixing chamber was calculated using the following equation

$$\lambda = \frac{|d\mathbf{x}|}{|d\mathbf{X}|} \tag{9}$$

A very small line segment $d\mathbf{X}$ of length $|d\mathbf{X}|$, given by $|d\mathbf{X}|/d \sim 10^{-6}$ and initial orientation vector $\mathbf{M}$, was advected for one period to its current length $|d\mathbf{x}|$ and orientation vector $\mathbf{m}$ (Ottino, 1989). About 3000 such initial locations $\mathbf{X}$, uniformly dispersed in the chamber, were considered for stretching calculations. Sample calculations with 10,000 initial locations produced identical distributions. The values of λ were averaged over 10 initial orientations at each initial location. Stretching ratios were calculated for five periods (23.5 s) of mixing with $\theta = 1440°$, such that the total strain γ was 207. Stretching ratios at higher strain were not calculated, as the trends became apparent at $\gamma = 207$. In addition, a small population of extended fibrils started to break up in experiments beyond this strain.

Results and Discussion

Poincaré maps and stretching distribution

Poincaré maps, presented in Figure 5, revealed very small islands near the rotors for sine waveform, which disappeared for square waveform and reappeared for the combined waveform. Note the symmetry of the Poincaré maps about the x-axis. Thus, the square waveform provided better distributive mixing than other waveforms, which is not surprising given that the same has been observed in earlier studies (Jana et al., 1994a; Leong and Ottino, 1989).

A better distributive mixing of fluid elements observed with square waveform can be rationalized in terms of length stretching ratios and their cumulative frequency distribution, presented in Figure 6. The narrowest distribution of stretching ratios is observed for steady motion of rotors, although the values are at least an order of magnitude smaller than the time-periodic waveforms. Among the time-periodic waveforms, the values of stretching ratios are observed to be the largest for the square waveform, followed by sine and combined waveforms. It can be seen from Figure 6 that approximately 80% of fluid elements experience stretching by a factor of 1.6×10^2, 7.9×10^3, 6.3×10^4, and 2.5×10^5, respectively, for steady, combined, sine, and square waveforms at a strain $\gamma = 207$. Such a dramatic difference is expected to have a strong impact on the speed of development of morphology, especially on the formation of the lamella from the molten domains of PP-phase and subsequent transformation of lamella into fibril and fibrils into droplets.

Some remarks are now in order on the relevance of stretching calculations to development of morphology of the PP-phase. A narrow stretching distribution means that a large fraction of the PP-phase experiences uniform stretching, leading to formation of lamellas with tight distribution of striation thicknesses. In addition, a higher value of stretching ratio in a given mixing time means faster reduction of the lamella thickness and a possibility of much earlier transition of the lamellas into fibrils. This also means larger stretching of the fibrils and faster transformation into droplets. It was found in the case of steady rotor motion that the stretching values are of the order of 100 for a total strain of 207 (Figure 6). One can anticipate the formation of thicker lamellas and larger diameter fibrils in this case, which may yield larger droplets and coarse final morphology.

The stretching values are much larger for square waveform, although with wider distribution. Consequently, faster deformation of the PP-phase into lamella is anticipated. However, the square waveform may not be a lucrative option from the perspective of subsequent morphology development. It is seen in Figure 3 that in a time period T, rotor A is in motion for a time $T/2$, whereas rotor B remains stationary. In turn, rotor B turns in the period $(T/2) < t \leq T$, with rotor A remaining stationary. In view of this, a larger diameter fibril stationed in zones closer to the stationary surfaces, such as rotor B while rotor A is in motion, may break up prematurely because of relaxation, resulting in larger droplets. It is known from prior work that the breakup of fibrils to droplets is facilitated in the zone of weak stretching (Kang et al., 1996; Tjahjadi and Ottino, 1991). A waveform, delivering continuous motion, to fibrils, such as a sine waveform, may delay their breakup because it offers higher stretching of lamella and fibrils through continuous motion of the rotors. The stretching distribution of the combined waveform, as expected, falls in between the steady case and sine waveform (Figure 6).

Morphology development

The optical images presented in Figure 7 reveal the existence of PP-phase in lamellar and fibrillar forms at various values of

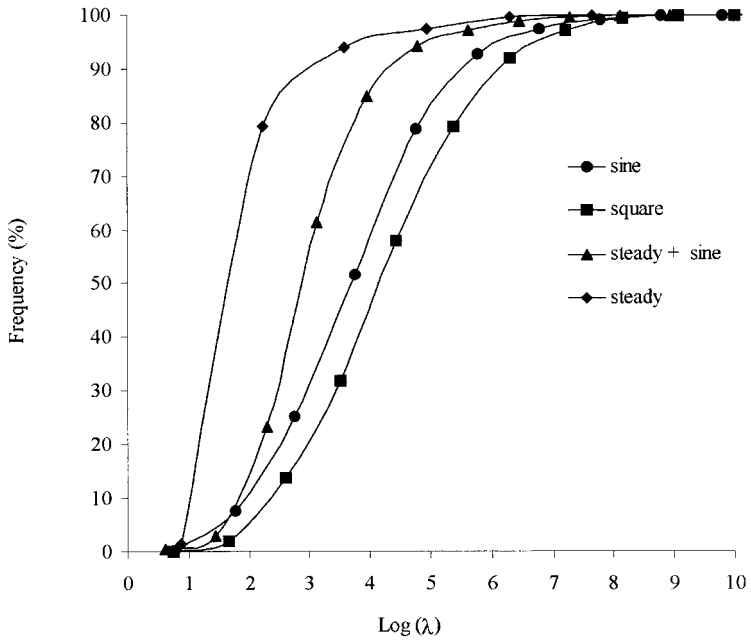

Figure 6. Cumulative distribution of stretching ratio for sine, square, and combined waveforms and steady rotor motion at a strain of 207.

strain (γ). In each case, the PA6-phase was extracted using formic acid. The fractions of the PP-phase converted into droplets were collected for further analysis. The weight fractions of the PP-phase remaining as lamellas and fibrils decrease with mixing time, as shown in Figure 8. It can be inferred from Figure 8 that the PP-phase converted most rapidly into droplets in the case of the sine waveform. For example, at a strain of 167, about 30% of the original PP-phase was converted into droplets with the sine waveform compared to 19, 10, and 5%, respectively, for the square waveform, combined waveform, and steady rotor motion. Additionally, as revealed in Figure 7, a large majority of the PP-phase converted into fine fibrils at a strain of 167 in the case of sine waveform, whereas mostly lamellas and some very thick fibrils are found for square waveform; mostly lamellas are also found in the case of combined waveform. In view of this, the rate of deformation of the PP-phase can be presented as follows: sine waveform > square waveform > combined waveform > steady motion.

The minimum, maximum, and number-average drop sizes at various values of strain (γ) for sine, square, and combined waveforms are shown in Table 1. The minimum droplet sizes fell in the same neighborhood, 0.5–3 μm, except for a 12-μm droplet in the case of the combined waveform. However, a striking contrast can be seen in a comparison of the maximum droplet sizes at each strain. For example, at a strain of 667, the largest droplet for the sine waveform was found to be 59 μm in diameter, whereas the square and combined waveforms produced the largest droplets of 259 and 265 μm diameter, respectively. As discussed earlier, this can be attributed to the premature breakup of large-diameter fibrils in the low stretching zones, such as near the stationary rotors in the case of the square waveform. It was later confirmed through separate an-

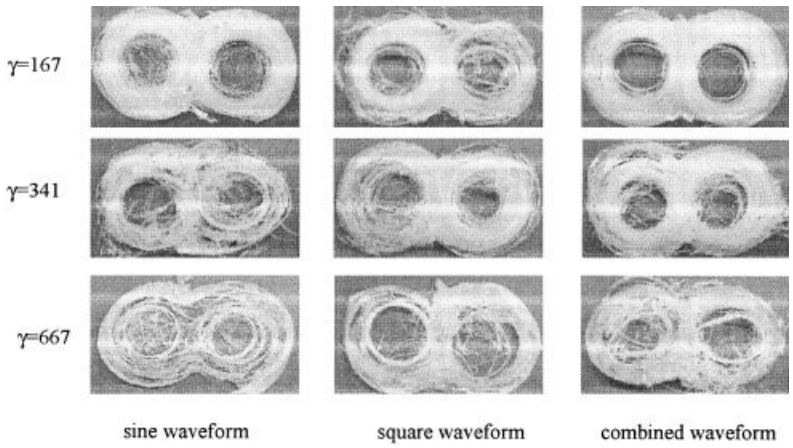

Figure 7. Optical images of layers and fibrils of PP-phase after extraction of PA6.

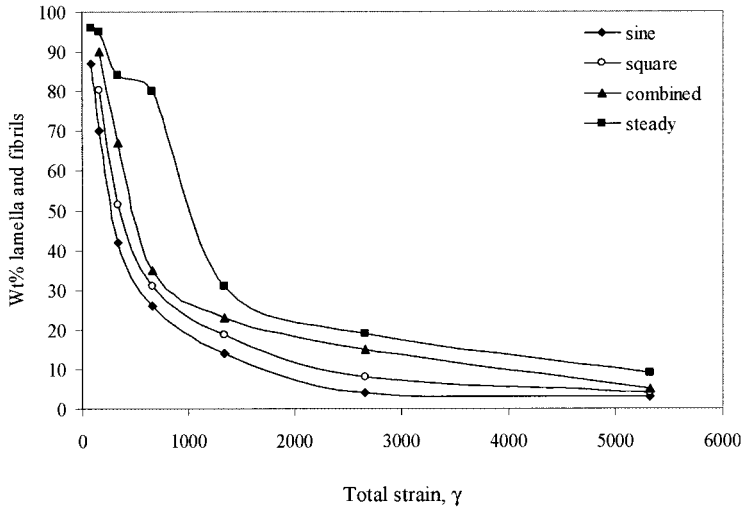

Figure 8. Weight percentage of the PP-phase in lamella and fibrillar forms with variation of strain (γ) for four waveforms.

nealing experiments that coalescence was not responsible at this stage for production of such large droplets (Jana and Sau, 2004; Sau, 2003).

The existence of very large droplets in the droplet population for square and combined waveforms is also reflected in the volume fraction of the droplets below and above the equilibrium diameter for this system (Table 2). The *equilibrium diameter* (d_{eq}) in this study corresponds to droplets that did not undergo further deformation once they were formed by coalescence from droplets of sizes smaller than d_{eq} and by breakup of droplets of sizes larger than d_{eq}. We used the Grace curve (see Figure 5 in Grace, 1982) for estimates of critical capillary number. For this purpose, the value of viscosity ratio was calculated to be 2.7 for the grades of PP and PA6 used in this study at a mean value of shear rate, 6.15 s^{-1}. The corresponding estimated critical capillary number was 7 and the value of d_{eq} was 78 μm. Note that the values of d_{eq} calculated from the critical capillary numbers represent the largest stable droplets.

These results showed that the volume percentage of the droplets falling below the equilibrium size for sine, square, combined, and steady waveforms are, respectively, 81, 33, 45, and 33% at a strain of 5320, even though >99% of the droplet populations fell below the equilibrium size in all cases. The sine waveform showed the highest volume fraction below the equilibrium size, attributed to faster deformation into thinner fibrils (Figure 8), which subsequently underwent breakup into smaller size droplets. Of the time-periodic waveforms, the smallest volume fraction below the equilibrium size was obtained in the case of combined waveform resulting from the presence of the steady speed component, which induced linear stretching of the dispersed phase and, therefore, did not contribute much to the exponential thinning of lamellas brought about by the sine wave time-periodic part. The number-average size of the fractions below the equilibrium size for sine and square waveform is found to be consistently about 1/4 of the equilibrium diameter.

The frequency distributions of the droplets are plotted in Figures 9 and 10 for the time-periodic waveforms for strain values of 1334 and 2662, respectively. The droplet diameters were first arranged in several bins of equal range of diameter. The mean volume of droplets in each bin and the number of droplets in each bin were recorded. The frequency distribution $f(V)$ was obtained such that $dN \equiv fdV$ droplets had volume between V and $V + dV$ in a population of N droplets. In each case, 1000–1500 droplets were used to generate the frequency distribution. The data presented in Figures 9 and 10 were scaled to 100 droplets. In general it is observed that the droplet sizes follow the order: sine wave < square wave < combined wave. A large population of droplets of much smaller volume can be seen in the case of the sine waveform, whereas the combined waveform produced droplets of larger size. The broadness of the distributions also follows the same order: sine wave < square wave < combined wave. Another interesting feature is the existence of a plateau in Figures 9 and 10, observed at lower volumes in the case of square and combined

Table 1. Minimum, Maximum, and Number-Average Droplet Diameters for Three Waveforms

	Sine Waveform			Square Waveform			Combined Waveform		
Total Strain (γ)	Min (μm)	Max (μm)	Number Average (μm)	Min (μm)	Max (μm)	Number Average (μm)	Min (μm)	Max (μm)	Number Average (μm)
167	2	324	51	3	388	29	12	468	74
341	0.5	243	23	0.7	234	18	1	256	20
667	0.8	59	8	1.5	259	14	1	265	23
1334	1.2	65	11	0.8	107	14	1	132	19
2662	1.3	112	13	1.3	259	15	0.7	198	17
5320	1	93	15	1.0	153	16	0.9	142	15

Table 2. Breakdown of Drops by Fraction by Volume and by Number below the Equilibrium Diameter of 78 μm Obtained with Various Waveforms

	Strain (γ)					
	167	334	667	1334	2662	5320
Fraction of droplets below equilibrium size (number/volume)						
Sine	0.8/0.003	0.91/0.001	1.0/1.0	1.0/1.0	0.999/0.82	0.997/0.81
Square	0.95/0.31	0.97/0.20	0.99/0.33	0.99/0.60	0.98/0.19	0.99/0.33
Combined	0.66/0.04	0.97/0.30	0.95/0.18		0.99/0.45	0.99/0.45
Steady	0.99/0.45	0.98/0.60	0.97/0.53	0.97/0.03	0.98/0.19	0.99/0.33
Number-average drop diameter of fractions below and above equilibrium (μm)						
Sine	36/111	16/111	8/—	11/—	12/112	16/105
Square	27/102	15/116	13/119	13/92	15/130	15/128
Combined	43/135	17/109	18/111		16/113	14/103
Steady	15/103	18/95	18/90	22/145	15/130	15/128

waves, which indicate multiple breakup of droplets formed early in mixing (Muzzio et al., 1991b).

The observed trends are in agreement with the findings of the stretching distribution reported in Figure 6. Because steady and combined waveforms produced lower stretching compared to that of sine and square waveforms, morphology development became slower in the former cases, as can be seen from the higher weight fractions of PP-phase remaining in lamellar and fibrillar forms as in Figure 8. The slower pathway of development also reflected in the number-average sizes observed for four waveforms in Table 2. The number-average PP domain size is the largest for the steady waveform and the smallest for the sine waveform. For example, at a strain of 1334, the number-average PP domain sizes for sine, square, and steady waveforms are 11, 13, and 22 μm, respectively.

The results of this study lead to two interesting questions. First, a practicing engineer, interested in developing a new chaotic mixing device or retrofitting existing ones, may ask a pertinent question about the ways of implementing a particular waveform, such as the sine waveform. It is demonstrated in this work and other studies in the literature (see, for example, Jana et al., 1994a; Swanson, 1991) that in batch mixing, time-periodic waveforms of an arbitrary form can be easily implemented and such batch mixing devices can be used to great advantage in product development studies or in making materials in moderate quantities. However, realization of a particular waveform—found so effective in batch mixing study—in continuous mixing devices poses a problem. First, it is desirable in a continuous mixing scheme that the screw-extrusion element rotates with a constant speed and, therefore, chaotic mixing must be introduced through spatial periodicity of fluid-element trajectories. Second, screw-element helices must be used to convey polymer melt and to develop enough head pressure, thus limiting the scope of alteration of the screw-

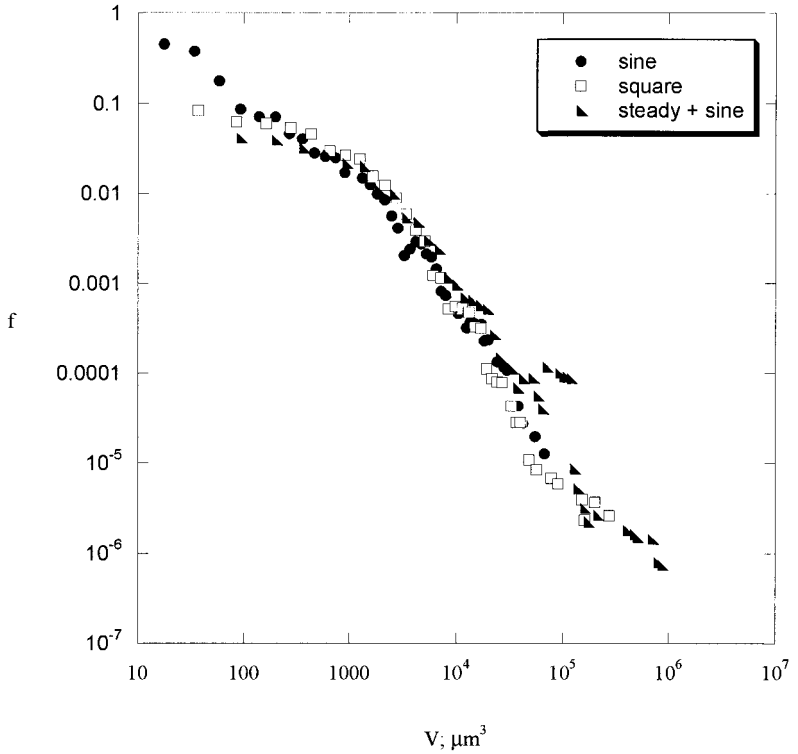

Figure 9. Frequency distribution of drop size for a strain (γ) of 1334 with three waveforms.

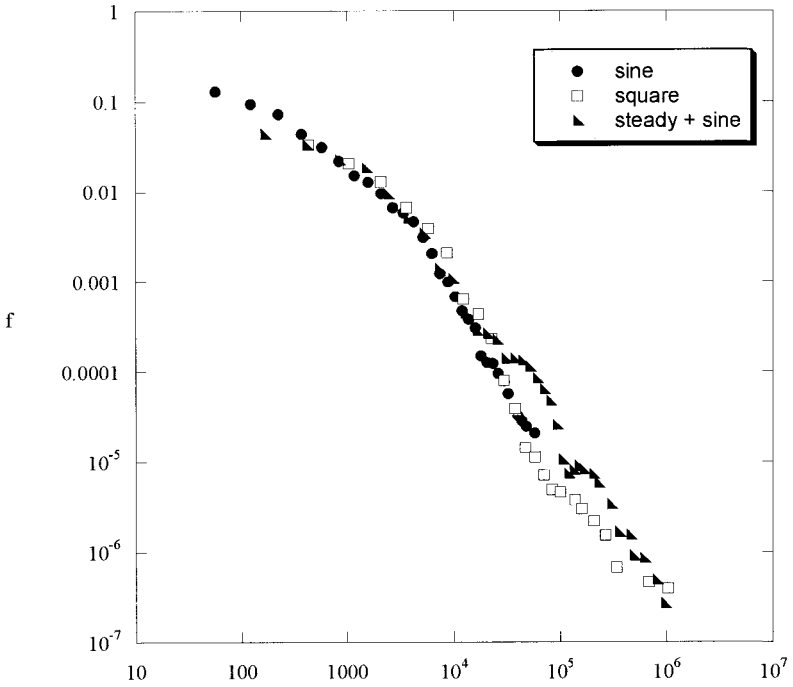

Figure 10. Frequency distribution of drop size for a strain (γ) of 2662 with three waveforms.

channel designs. Third, any such modification may produce a convoluted waveform, instead of the desired single-frequency waveform. Figure 11 presents a sketch of a single extruder screw that produces continuous chaotic mixing through periodic alteration of screw-channel geometry, which was developed for blending of immiscible polymers (Jana, 2002; Jana et al., 2000). In this case, the speeds of fluid elements follow convoluted waveforms as they travel down the flow channel. Recently, a study reported the use of a continuous chaotic mixing device, whereby molten component polymers were fed into a channel under head pressure and mixed by time-periodic square waveform motion of two circular rotors (Zumbrunnen and Inamdar, 2001).

The second important question relates to determination of the degree of chaotic mixing, if present at all, in conventional screw extruders and mixing devices. It is clear that some degree of chaotic mixing is present in twin-screw extrusion systems, given that instantaneous streamline portraits from the motion of kneading blocks and screw elements show appreciable crossing. Some studies also reported the existence of chaotic fluid-element trajectories in the kneading zones of intermeshing corotating twin-screw extruders (Cheng and Manas-Zloczower, 1997, 1998; Kalyon and Sangani, 1989). However, no attempt has been made in these studies to assess the degree of chaotic mixing. In addition, studies on quantitative comparison of blending by screw extrusion and chaotic mixing under the same conditions of shear rates are still lacking.

A future study on chaotic mixing should consider shear rates in the range of 50–100 s^{-1}. Although the peak shear rate used in this study, 17.7 s^{-1}, was much less than the peak shear rates of typically 100 s^{-1} found in screw extruders, such lower shear rates provided opportunities to observe the various stages of morphological development. Our limited effort to carry out experiments at peak shear rates of about 50 s^{-1} led to development of normal stresses, which caused frequent misalignment of the rotors. A new mixing device has been built in our laboratory to carry out experiments at shear rates of 100–150 s^{-1}, the results of which will be reported in the future.

Concluding Remarks

The results presented herein show that the nature of waveforms affects the rate of morphology development, the morphological makeup, and the size distribution of droplets. It is seen from the Poincaré map in Figure 5 that the square waveform gives rise to better distributive mixing, although during mixing of PP with PA6, some very large size droplets were generated. In this case, the large-size droplets from early breakup and smaller droplets formed in the high stretching

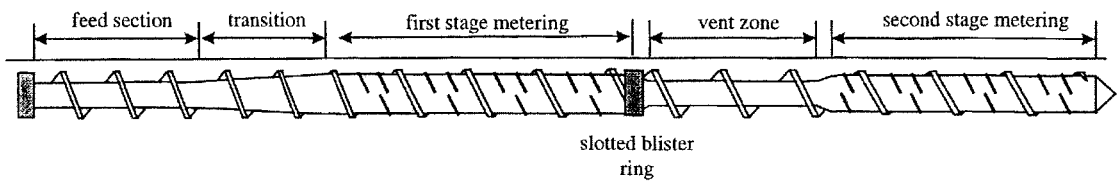

Figure 11. Single-screw extruder that produces chaotic mixing of miscible and immiscible polymer components.

zones, such as near the rotors in motion, led to broader size distribution. The sine waveform, providing continuous stretching of fibrils, produced the fastest deformation of the PP-phase into lamellas, fibrils, and droplets compared with other waveforms.

Acknowledgments

This work was supported by National Science Foundation in the form of a CAREER Award (DMI-0134106) to S.C.J.

Literature Cited

Aref, H., "Stirring by Chaotic Advection," *J. Fluid Mech.*, **143**, 1 (1984).
Chappelear, D. C., "Interfacial Tension between Molten Polymers," *Polym. Prepr.* (*Am. Chem. Soc., Div. Polym. Chem.*), **5**, 363 (1964).
Cheng, H., and I. Manas-Zloczower, "Chaotic Features of Flow in Polymer Processing Equipment. Relevance to Distributive Mixing," *Int. Polym. Proc.*, **12**, 83 (1997).
Cheng, H., and I. Manas-Zloczower, "Distributive mIxing in Conveying Elements of a ZSK-53 Co-Rotating Twin Screw Extruder," *Polym. Eng. Sci.*, **38**, 926 (1998).
Chesters, A., "The Modeling of Coalescence Processes in Fluid–Liquid Dispersions: A Review of Current Understanding," *Chem. Eng. Res. Des.*, **69A**, 259 (1991).
Chien, W.-L., H. Rising, and J. M. Ottino, "Laminar Mixing and Chaotic Mixing in Several Cavity Flows," *J. Fluid. Mech.*, **170**, 355 (1986).
Elemans, P. H. M., J. M. H. Janssen, and H. E. H. Meijer, "The Measurement of Interfacial Tension in Polymer/Polymer Systems: The Breaking Thread Method," *J. Rheol.*, **34**, 1311 (1990).
Erwin, L., "Theory of Laminar Mixing," *Polym. Eng. Sci.*, **18**, 1044 (1978a).
Erwin, L., "Theory of Mixing Sections in Single Screw Extruders," *Polym. Eng. Sci.*, **18**, 572 (1978b).
Galaktionov, O. S., P. D. Anderson, G. W. M. Peters, and C. L. Tucker III, "A Global, Multi-Scale Simulation of Laminar Fluid Mixing: The Extended Mapping Method," *Int. J. Multiphase Flow*, **28**, 497 (2002).
Ghosh, A., S. Ranganathan, J. T. Lindt, and S. Lorex, "Blend Morphology Development in a Single Screw Extruder," *Proc. of SPE ANTEC 1991*, pp. 232–236 (1991).
Grace, H. P., "Dispersion Phenomena in High Viscosity Immiscible Fluid Systems and Application of Static Mixers as Dispersion Devices in Such Systems," *Chem. Eng. Commun.*, **14**, 225 (1982).
Higdon, J. J. L., "Stokes Flow in Arbitrary Two-Dimensional Domains: Shear Flow over Ridges and Cavities," *J. Fluid Mech.*, **159**, 194 (1985).
Jana, S. C., "Avenues of Introducing Chaotic Mixing in Single-Screw Extruders," *Proc. SPE ANTEC*, **60**, 1436 (2002).
Jana, S. C., G. Metcalfe, and J. M. Ottino, "Experimental and Computational Studies of Mixing in Complex Stokes Flows: The Vortex Mixing Flow and Multicellular Cavity Flows," *J Fluid Mech.*, **269**, 199 (1994a).
Jana, S. C., and M. Sau, "Effects of Viscosity Ratio and Composition on Development of Morphology in Chaotic Mixing of Polymers," *Polymer*, **45**, 1665 (2004).
Jana, S. C., E. Scott, and U. T. Sundararaj, "Single Extruder Screw for Blending of Miscible and Immiscible Polymeric Materials," U.S. Patent No. 6 132 076 (2000).
Jana, S. C., M. Tjahjadi, and J. M. Ottino, "Chaotic Mixing of Viscous Fluids by Periodic Changes in Geometry: The Baffled Cavity Flow," *AIChE J.*, **40**, 1769 (1994b).
Jenssen, J. M. H., and H. E. H. Meijer, "Dynamics of Liquid–Liquid Mixing: A 2-Zone Model," *Polym. Eng. Sci.*, **35**, 1766 (1995).
Jones, S. W., O. M. Thomas, and H. Aref, "Chaotic Advection by Laminar Flow in a Twisted Pipe," *J Fluid Mech.*, **209**, 335 (1989).
Kalyon, D. M., and H. N. Sangani, "An Experimental Study of Distributive Mixing in Fully Intermeshing, Co-Rotating Twin-Screw Extruders," *Polym. Eng. Sci.*, **29**, 1018 (1989).
Kang, J., T. G. Smith, and D. I. Bigio, "Study of Breakup Mechanisms in Cavity Flow," *AIChE J.*, **42**, 649 (1996).
Kaper, T. J., and S. Wiggins, "An Analytical Study of Transport in Stokes Flows Exhibiting Large-Scale Chaos in the Eccentric Journal Bearing," *J. Fluid Mech.*, **253**, 211 (1993).
Kim, S. J., and T. H. Kwon, "Enhancement of Mixing Performance of Single-Screw Extrusion Processes via Chaotic Flows. Part I. Basic Concepts and Experimental Study," *Adv Polym Technol.*, **15**, 41 (1996a).
Kim, S. J., and T. H. Kwon, "Enhancement of Mixing Performance of Single-Screw Extrusion Processes via Chaotic Flows. Part II. Basic Concepts and Experimental study," *Adv Polym Technol.*, **15**, 55 (1996b).
Kruijt, P. G. M., O. S. Galaktionov, P. D. Anderson, G. W. M. Peters, and H. E. H. Meijer, "Analyzing Mixing in Periodic Flows by Distribution Matrices: Mapping Method," *AIChE J.*, **47**, 1005 (2001).
Kusch, H. A., and J. M. Ottino, "Experiments on Mixing in Continuous Chaotic Flows," *J. Fluid Mech.*, **236**, 319 (1992).
Kwon, O., and D. A. Zumbrunnen, "Progressive Morphology Development to Produce Multilayer Films and Interpenetrating Blends by Chaotic Mixing," *J. Appl. Polym. Sci.*, **82**, 1569 (2001).
Leong, C. W., and J. M. Ottino, "Experiments on Mixing Due to Chaotic Advection in a Cavity," *J. Fluid. Mech.*, **209**, 463 (1989).
Lindt, J. T., and A. K. Ghosh, "Fluid Mechanics of Formation of Polymer Blends. Part I. Formation of Lamellar Structure," *Polym. Eng. Sci.*, **32**, 1802 (1992).
Liu, Y. H., and D. A. Zumbrunnen, "Toughness Enhancement in Polymer Blends Due to the In-Situ Formation by Chaotic Mixing of Fine-Scale Extended Structures," *J. Mater. Sci.*, **34**, 1921 (1999).
Lyngaae-Jorgensen, J., "Experimental Methods for In Situ Studies of Morphology Development during Flow: The Case of Instability of Thin Films Studied by Light Scattering," *J. Macromol. Sci. Phys.*, **B35**, 357 (1996).
Metcalfe, G., and J. M. Ottino, "Autocatalytic Processes in Mixing Flows," *Phys. Rev. Lett.*, **72**, 2875 (1994).
Muzzio, F. J., and M. Liu, "Chemical Reactions in Chaotic Flows," *Chem. Eng. J.*, **64**, 117 (1996).
Muzzio, F. J., P. D. Swanson, and J. M. Ottino, "The Statistics of Stretching and Stirring in Chaotic Flows," *Phys. Fluids A*, **3**, 822 (1991a).
Muzzio, F. J., M. Tjahjadi, and J. M. Ottino, "Self-Similar Drop-Size Distributions Produced by Breakup in Chaotic Flows," *Phys Rev Lett.*, **67**, 54 (1991b).
Niederkorn, T. C., and J. M. Ottino, "Mixing of a Viscoelastic Fluid in a Time-Periodic Flow," *J. Fluid Mech.*, **256**, 243 (1993).
Ottino, J. M., *The Kinematics of Mixing: Stretching, Chaos, and Transport*, Cambridge Univ. Press, New York (1989).
Ottino, J. M., W. E. Ranz, and C. W. Macosko, "A Lamellar Model for Analysis of Liquid–Liquid Mixing," *Chem. Eng. Sci.*, **34**, 877 (1979).
Sau, M., "Morphology Development in Chaotic Mixing of Polymers," PhD Thesis, University of Akron, Akron, OH (2003).
Sau, M., and S. C. Jana, "A Study on the Effects of Chaotic Mixer Design and Operating Conditions on Morphology Development in Immiscible Polymer Systems," *Polym. Eng. Sci.*, **44**, 407 (2004); Errata: 44, 1403 (2004).
Scott, C. E., and C. W. Macosko, "Model Experiments Concerning Morphology Development during the Initial Stages of Polymer Blending," *Polym. Bull.*, **26**, 341 (1991).
Scott, C. E., and C. W. Macosko, "Morphology Development during the Initial Stages of Polymer–Polymer Blending," *Polymer*, **36**, 461 (1995).
Sundararaj, U., Y. Dori, and C. W. Macosko, "Sheet Formation in Immiscible Polymer Blends: Model Experiments on Initial Blend Morphology," *Polymer*, **36**, 1957 (1995).
Sundararaj, U., C. W. Macosko, R. J. Rolando, and H. T. Chan, "Morphology Development in Polymer Blends," *Polym. Eng. Sci.*, **32**, 1814 (1992).
Swanson, P. D., "Regular and Chaotic Mixing of Viscous Fluids in Eccentric Rotating Cylinders," PhD Thesis, University of Massachusetts, Amherst (1991).
Swanson, P. D., and J. M. Ottino, "A Comparative Computational and Experimental Study of Chaotic Mixing of Viscous Fluids," *J. Fluid Mech.*, **213**, 227 (1990).
Szalai, E. S., J. Kukura, P. E. Arratia, and F. J. Muzzio, "Effect of Hydrodynamics on Reactive Mixing in Laminar Flows," *AIChE J.*, **49**, 168 (2003).

Tjahjadi, M., and J. M. Ottino, "Stretching and Breakup of Droplets in Chaotic Flows," *J. Fluid Mech.*, **232**, 191 (1991).
Vanoene, H., "Models of Dispersion of Viscoelastic Fluids in Flow," *J. Colloid Interface Sci.*, **40**, 448 (1972).
Zumbrunnen, D. A., and C. Chhiber, "Morphology Development in Polymer Blends Produced by Chaotic Mixing at Various Compositions," *Polymer*, **43**, 3267 (2002).
Zumbrunnen, D. A., and S. Inamdar, "Novel Sub-Micron Highly Multi-Layered Polymer Films Formed by Continuous Flow Chaotic Mixing," *Chem. Eng. Sci.*, **56**, 3893 (2001).
Zumbrunnen, D. A., K. C. Miles, and Y. H. Liu, "Auto-Processing of Very Fine-Scale Composite Materials by Chaotic Mixing of Melts," *Composites Part A*, **27A**, 37 (1996).

Manuscript received Jun. 11, 2003, and revision received Jan. 11, 2004.